KSOE

Journal of Ocean Engineering and Technology 38(5), 257-268, October, 2024
https://doi.org/10.26748/KSOE.2024.050

pISSN 1225-0767
eISSN 2287-6715

Original Research Article

Thermodynamic Modeling and Analysis of Boil-off Gas Generation and Self-Pressurization in Liquefied Carbon Dioxide Tanks

Taehun Nam[1], Taejong Yu[1] and Youngsub Lim[2]

[1]*Graduate student, Department of Naval Architecture and Ocean Engineering, Seoul National University, Korea*
[2]*Professor, Department of Naval Architecture and Ocean Engineering, Seoul National University, Korea*

KEYWORDS: Boil-off gas, LCO_2, Self-pressurization, Thermodynamic model

ABSTRACT: *The importance of the safe transport of liquefied carbon dioxide (LCO_2) is increasing owing to environmental issues. When transporting a low-temperature liquid, boil-off gas generation and self-pressurization occur due to heat ingress, affecting the holding time of a low-temperature liquid tank. This study developed and compared three thermodynamic self-pressurization models to estimate the holding time of LCO_2: Thermal homogeneous model (THM), Thermal two-zone model (TTZM), and Thermal multi-zone model (TMZM). Thermodynamic differential equations were solved for THM, and software was used for TTZM. For TMZM, the parameters were optimized using experimental data to determine the heat ratio parameter f and heat transfer parameters K_1 and K_2. THM and TTZM estimated an unreasonably long holding time, approximately 42 days. The TMZM, however, showed a satisfactory holding time of 12–13 days. These results can help predict the self-pressurization in the storage tanks of LCO_2 and be applied to actual LCO_2 carrier cargo handling systems, with the modeling results indicating that the 12–13 days of LCO_2 self-pressurization based on the TMZM appears to be the most suitable.*

Nomenclature

Variables

m	mass
$\dot{m}$	mass flow rate
T	temperature
P	pressure
t	time
ρ	density
h	enthalpy
Q	heat
L	characteristic length
C_s	specific heat capacity
C_p	specific heat at constant pressure
K_1	heat transfer factor between vapor to surface
K_2	heat transfer factor between surface to liquid
$\dot{Q}$	heat flow
V	volume
A	area
λ	thermal conductivity
f	heat ratio factor
α	heat transfer coefficient
β	Thermal expansion coefficient

Subscripts

f	filling ratio
in	inlet
out	outlet
s	saturation (or surface)
v	vapor
l	liquid
vl	vapor to liquid
vs	vapor to surface
sl	surface to liquid
Ra	Rayleigh number
Pr	Prandtl number
N	Nusselt number
i	initial
e	end

Received 3 April 2024, revised 23 July 2024, accepted 10 September 2024
Corresponding author Youngsub Lim: +82-2-880-7325, s98thesb@snu.ac.kr

1. Introduction

Serious climate change issues have increased research interest in carbon capture and storage (CCS) technology to reduce greenhouse gas (GHG) emissions. Various technologies, such as efficiency improvement and the use of alternative fuels, have been discussed to reduce GHG emissions. On the other hand, efficiency improvement technologies cannot avoid fundamental carbon generation, and alternative fuels still have insufficient mass production infrastructure to meet global demand. Therefore, the application of CCS technology that is immediately applicable has been discussed (Jung and Seo, 2022). Various systems can be considered for carbon capture, but the chemical absorption method that uses amine solutions has been used most widely owing to the high technological maturity and many application cases (Kearns et al., 2021). In general, captured carbon dioxide is liquefied, transported to areas with infrastructure, and stored in isolation. For example, Norway's Sleipner project has been storing carbon dioxide by injecting it into a saline aquifer at the sub-bottom of 3,500 m (Kongsjorden et al., 1998). In Iceland, efforts have been made to develop carbon-neutral technologies and establish a Coda terminal, a carbon dioxide storage terminal, through the Carbfix project (Clark et al., 2020).

Carbon dioxide storage and transport technologies through ships should be considered for the application of CCS technology. International mass transport problems occur when captured carbon dioxide is transported to areas where it can be stored because areas with large storage facilities are limited. Therefore, more attention has been paid to CO_2 transport by sea. For large-capacity CO_2 transport by sea, liquefied CO_2 (LCO_2) is usually stored in the internal tanks of ships. Higher pressures than room temperature and low-temperature storage conditions are required because CO_2 has a triple point of 520 kPa and 56.6 ℃. Conventional LCO_2 carriers generally have transport conditions of 1,000 to 1,500 m^3 and 1,400 to 2,000 kPa (Hegerland et al., 2005). This requires high-pressure storage tanks. Hence, it is unfavorable in terms of cost for large-capacity CO_2 transport. Therefore, transport of LCO_2 at a low pressure of approximately 650 kPa has been considered (Aspelund et al., 2006). IMO tank type C, which can withstand pressures of up to 800 to 1,000 kPa, is suitable for LCO_2 stored under these conditions, and a study was conducted on large-capacity CO_2 transport using vertical-type double cylinder (Bi-lobe) tanks considering the cargo capacity and hull shape (Cheon et al., 2023).

Regarding storage tanks for low-temperature liquids below room temperature, the impact of boil-off gas (BOG) caused by heat ingress must be considered. The generation and accumulation of BOG in a tank with limited volume cause an increase in pressure inside the tank. Damage to related equipment and the discharge of the stored fluid can occur if the internal pressure exceeds the maximum allowable working pressure of the tank. Hence, many studies have been conducted on predicting self-pressurization in cryogenic liquid storage tanks. In the case of liquid hydrogen (LH_2), the self-pressurization experiment results showed that the pressure increased rapidly from 117 kPa at the beginning to 180 kPa after approximately 20 h, and the pressure rise rate also varied according to the level inside the LH_2 tank (Barsi and Kassemi, 2008). In the case of liquid nitrogen, a pressure rise of 20 kPa for approximately 1 h was observed due to the external heat of 1.2 kW, and its rate was affected by the magnitude of external heat (Seo and Jeong, 2010). In the case of LNG storage tanks, pressure increase rates of 120, 145, and 232 kPa/d were observed at levels of 15, 50, and 85%, respectively, which shows that the pressure increase rate increases as the level increases (Kim et al., 2024). In the case of LCO_2, the pressure rise by BOG is expected, and its prediction is important for safe carbon dioxide transport.

Various studies have also been conducted on predictive models based on thermodynamic models that predict the self-pressurization rate. The predictive models can be divided into four types. The first is the thermal homogeneous model (THM), which assumes that gas and liquid maintain an equilibrium state with the same temperature and pressure. Peng and Ahluwalia (2013) simulated the internal pressure rise of a small-capacity liquefied hydrogen tank by external heat through the application of an equilibrium model in which liquid and gas are in the same saturation state. They reported a 42-day self-pressurization period in the model simulation results for a 151 L tank with a maximum allowable working pressure of 34 Mpa. Nevertheless, a non-equilibrium state with different temperature distributions from the top to the bottom of the tank occurs as the size of

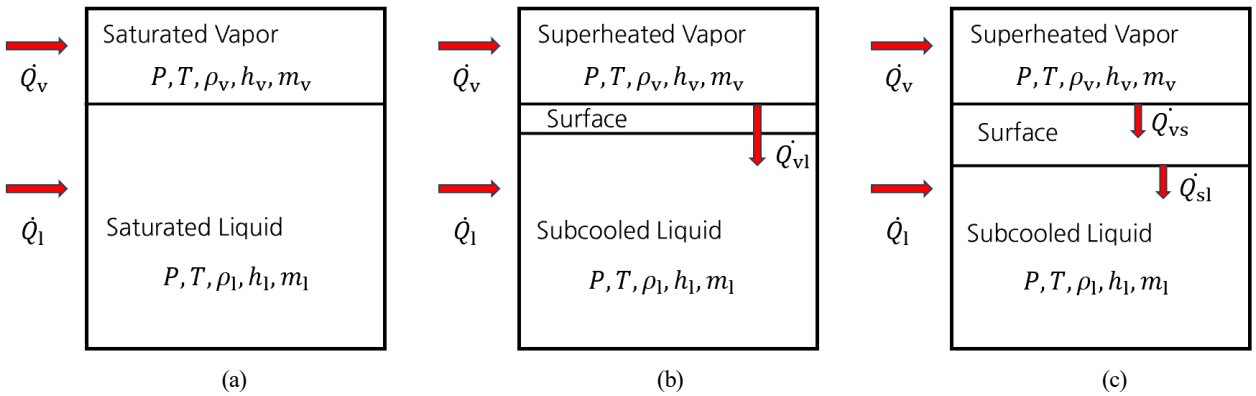

Fig. 1 Conceptual schematic diagram of the cryogenic tank using THM (a), TTZM (b), and TMZM (c)

the tank increases because of heat transfer inside the tank, which may exhibit different behavior from the equilibrium state. Studies have also been conducted to simulate this non-equilibrium state using the thermal two-zone model (TTZM) that distinguished the regions of liquid and gas, which is the second type, and the thermal multi-zone model (TMZM), which is the third type. The TTZM assumes that the liquid is saturated while the gas is superheated vapor. TMZM reflects realistic heat exchange between the liquid and gas using three or more regions, including subcooled, superheated, and saturated regions. Fig. 1 presents the schematics of these models.

Al Ghafri et al. (2022) evaluated the prediction of self-pressurization of liquefied hydrogen using TTZM, a non-equilibrium model. They performed simulations by reflecting the heat exchange between the liquid and gas and verified its effectiveness through a comparison with the results of the liquefied hydrogen experiment. Wang et al. (2022) applied the TMZM to predict the self-pressurization of liquefied hydrogen using the results of the multipurpose hydrogen test bed (MHTB) experiment performed by Hastings et al. (2003). They reported changes in pressure rise rate according to the previous THM and experiment results and the difference in external heat as shown in Fig. 2. Matveev and Leachman (2023) presented the difference in velocity changes according to the size of the liquefied hydrogen tank and the volume of the liquid using TMZM. Most of these studies, however, were limited to small-capacity tanks and could not present the results for large-capacity tanks. As the final type, modeling and simulation studies have been conducted using CFD. Studies that used CFD presented the self-pressurization results of liquefied hydrogen based on phase change models (Kartuzova et al., 2014). Research has been conducted on various cryogenic substances, including LNG and nitrogen, rather than liquefied hydrogen (Seo and Jeong, 2010; Zhu et al., 2020). Most of the studies that used CFD utilized models, such as the thermal diffusion model (TDM) and the kinetic theory of gas model (KTG), and such modeling required many calculations.

For LCO_2, self-pressurization also occurs because of the occurrence of BOG caused by external heat under the storage condition of −52 ℃. In the case of LNG, the substances contained in LNG have different evaporation rates because LNG is a mixture and is mainly stored and transported at 100 kPa, which is the ambient pressure condition, and −162 ℃. In the case of liquefied hydrogen, very high insulation conditions (e.g., vacuum insulation) are required because of the ambient pressure cryogenic temperature (20 K). In the case of LCO_2, a storage pressure condition of more than medium pressure (at least 600 kPa) is required because of the high triple point, and the prediction of self-pressurization is essential because the pressure difference from the maximum allowable working pressure of the tank is small. Therefore, this study developed a model for the internal pressure rise of LCO_2 based on thermodynamic models and predicted the degree of the pressure rise through simulation. Equilibrium and non-equilibrium models that are classified according to the vapor−liquid state inside the tank were implemented using the Python code, and Aspen Hysys was utilized as the database for thermodynamic properties. The simulation model was verified by optimizing the parameters in the model and comparing the results of previous LCO_2 tank experiments. The results of the simulation on self-pressurization prediction were presented based on this and the actual operating conditions of LCO_2 storage tanks.

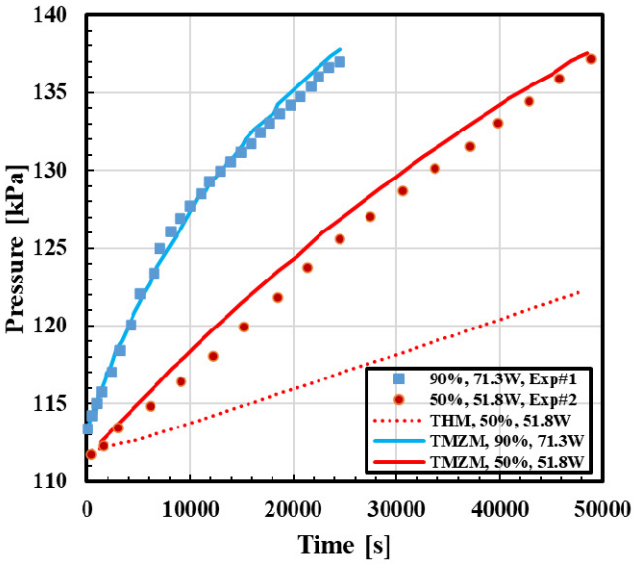

Fig. 2 Comparison of the pressure curves between two models against the experiments (Modified from Wang et al., 2022)

2. Background Knowledge

2.1 Thermodynamic Models

2.1.1 THM (Thermal homogeneous model)

An equilibrium model assumes that the liquid and gas inside the tank are in complete equilibrium. Rotenberg et al. (1986) described the pressure increase modeling by the occurrence of BOG inside the tank during the isochoric process using THM, an equilibrium model. In the tank where low-temperature fluid is stored, constant external heat ($\dot{Q}_{in}$) per hour is introduced, resulting in temperature changes and pressure increases. Assuming no external mass flow-in and a steady state in the tank, the pressure change inside the tank can be calculated from the calculation of the internal temperature change caused by external heat (Peng and Ahluwalia, 2013). These are expressed in Eqs. (1) to (3).

$$\frac{dm_{CO_2}}{dt} = \dot{m}_{CO_2}^{in} - \dot{m}_{CO_2}^{out} = 0 \tag{1}$$

$$\left(m_s C_s + m_v\left[\left(\frac{\partial h_v}{\partial T}\right)_P\right] + m_l\left[\left(\frac{\partial h_l}{\partial T}\right)_P\right] + \left(m_v\left[\left(\frac{\partial h_v}{\partial P}\right)_T\right] + m_l\left[\left(\frac{\partial h_l}{\partial P}\right)_T\right] - V\right)\frac{dP_s}{dT}\right)\frac{dT}{dt}$$
$$= (h_l - h_v)\frac{dm_v}{dt} + \dot{Q}_{in} = 0 \tag{2}$$

$$\frac{dP}{dt} = \frac{dP_s}{dT}\left(\frac{dT}{dt}\right) \tag{3}$$

2.1.2 TTZM (Thermal two-zone model)

The heat exchange between them in the tank where the actual liquid cargo is stored is not considered to evaluate the influence of heat and mass transfer because the liquid and gas are in the same saturated state in an equilibrium model (Wang et al., 2022). Al Ghafri et al. (2022) presented a model that enables heat transfer from the gas to the liquid in which the liquid has a uniform temperature distribution; the thermodynamic equilibrium state is considered in the interface region assumed as a very thin membrane, and the gas has a higher temperature than the liquid as superheated vapor. UWA (Jusko et al., 2021) released the BoilFAST software that can perform simulation by selecting the geometry, thermodynamic model, boundary conditions, and composition of the tank (Fig. 1(b)) and identify the BOG and self-pressurization of various fluids, including LCO_2, by applying TTZM (Al Ghafri et al., 2022).

2.1.3 TMZM (Thermal multi-zone model)

In the actual low-temperature liquid storage tank, superheated vapor, saturated phase equilibrium interface, and subcooled liquid have different temperature distributions, and each region can be explained using the average temperature to simplify the heat distribution inside the tank (Wang et al., 2022). Fig. 1(c) describes a TMZM-based tank with these three regions. Eqs. (4) to (6) are the energy balance equations of the gas, interface, and liquid, respectively (Wang et al., 2022).

$$\frac{d(\rho_v h_v V_v)}{dt} = Q_v - Q_{vs} + \dot{m}_{in} h_{s,v} \tag{4}$$

$$Q_{vs} - Q_{sl} = \dot{m}_{in}(h_v - h_{s,l}) \tag{5}$$

$$\frac{d(\rho_l h_l V_l)}{dt} = Q_l + Q_{sl} - \dot{m}_{in} h_{s,l} \tag{6}$$

Q_{vs} is the heat transfer rate between the gas and the interface, and Q_{sl} is the heat transfer rate between the interface and the liquid. These are induced by the multiplication of the temperature differences between each region and the area of the interface, as expressed in Eqs. (7) and (8) (Wang et al., 2022):

$$Q_{vs} = \alpha_{vs} A_{vs} (T_v - T_s) \tag{7}$$

$$Q_{sl} = \alpha_{sl} A_{sl} (T_s - T_l) \tag{8}$$

According to Zuo et al. (2021), the previous approach that reflects the heat transfer at the interface overestimated the amount of heat introduced into the gas, resulting in a problem that the temperature and pressure of the gas increase more rapidly than observed in reality. Wang et al. (2022) addressed this problem by introducing a parameter (f) for adjusting the heat transfer rate between the gas and the liquid:

$$f = \frac{Q_v / A_v}{Q_l / A_l} = \frac{q_v}{q_l} \tag{9}$$

$$Q_v = q_v A_v \tag{10}$$

$$Q_l = q_l A_l \tag{11}$$

α_{vs} and α_{sl} are the heat transfer coefficients, corresponding to Eqs. (12) and (13) (Wang et al., 2022), according to Holman (2002) and Nellis and Klein (2009). K_1 and K_2 are the parameters that correct the magnitude of the heat transfer rate between the interfaces.

$$\alpha_{vs} = 0.27 \times K_1 \frac{\lambda}{L} \times Ra^{0.25} \tag{12}$$

$$\alpha_{sl} = 2.5 \times K_2 \frac{\lambda}{L} \left\{ \ln \left\{ 1 + \frac{2.5}{0.527 \times Ra^{0.2}} \times \left[1 + \left(\frac{1.9}{\mathrm{Pr}} \right)^{0.9} \right]^{\frac{2}{9}} \right\} \right\}^{-1} \tag{13}$$

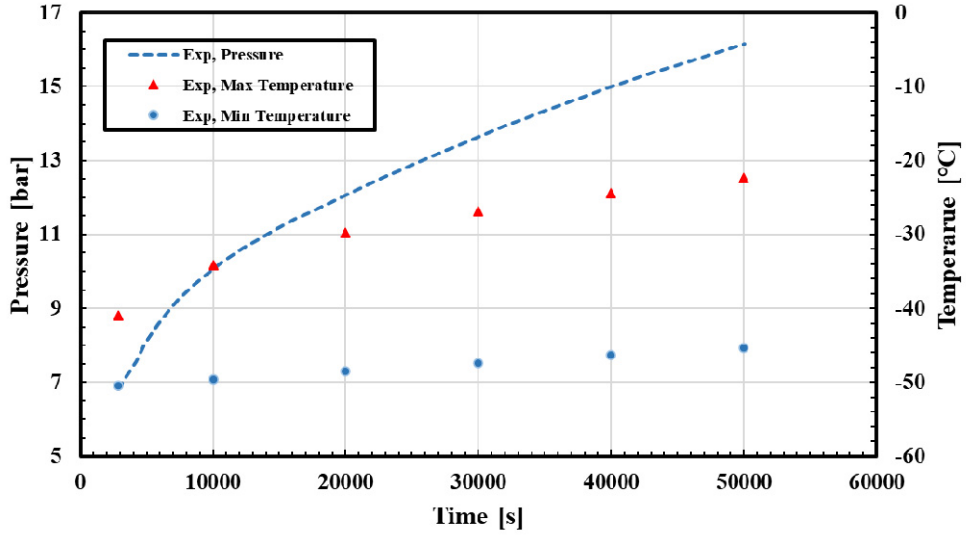

Fig. 3 Pressure increasing in the experiment (Yoo, 2011)

2.2 LCO_2 Tank Experiment

Yoo (2011) performed a tank experiment with a high filling ratio and initial storage pressure (682 kPa) for research on LCO_2 carriers; 99.99% LCO_2 close to a pure substance was placed at room temperature, and self-pressurization and the temperature of each layer were measured. A vertical cylinder tank designed to withstand up to 3,000 kPa was used in the experiment. The experimental results revealed a pressure increase rate of 168 kPa/h to 10,000 s and a pressure increase rate of 50 kPa/h from 20,000 s to 50,000 s (Fig. 3), indicating that the pressure increase rate decreased with a 118 kPa/h difference. In addition, the difference between the maximum and minimum temperatures during the same period increased gradually, resulting in a temperature difference of 23 K at 50,000 s. Table 1 and Fig. 4 show the specifications and geometry of the tank used in the experiment, respectively. Fig. 5 shows the pressure-temperature diagram of pure carbon dioxide.

Table 1 Dimensions and test conditions of a cargo tank (Yoo, 2011)

Parameter	Value
Internal height (mm)	2,450
Internal diameter (mm)	1,036
Tank thickness (mm)	18
Filing ratio	0.96
Initial pressure (kPa)	682
Insulation material	PUF, Al
Insulation thickness (mm)	150
Thermal conductivity (W/m K)	0.026

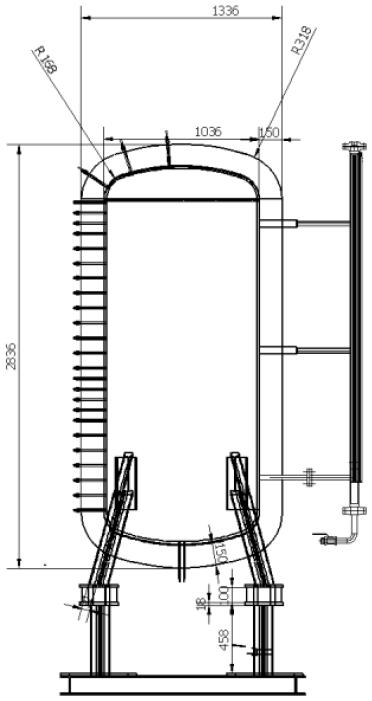

Fig. 4 Cargo tank drawing in the experiment (Yoo, 2011)

3. Modeling and Simulation

3.1 Modeling

Expressions for temporal changes must be considered in self-pressurization simulations. In this study, a model was developed using Python code for thermodynamic calculations, such as mass flow and

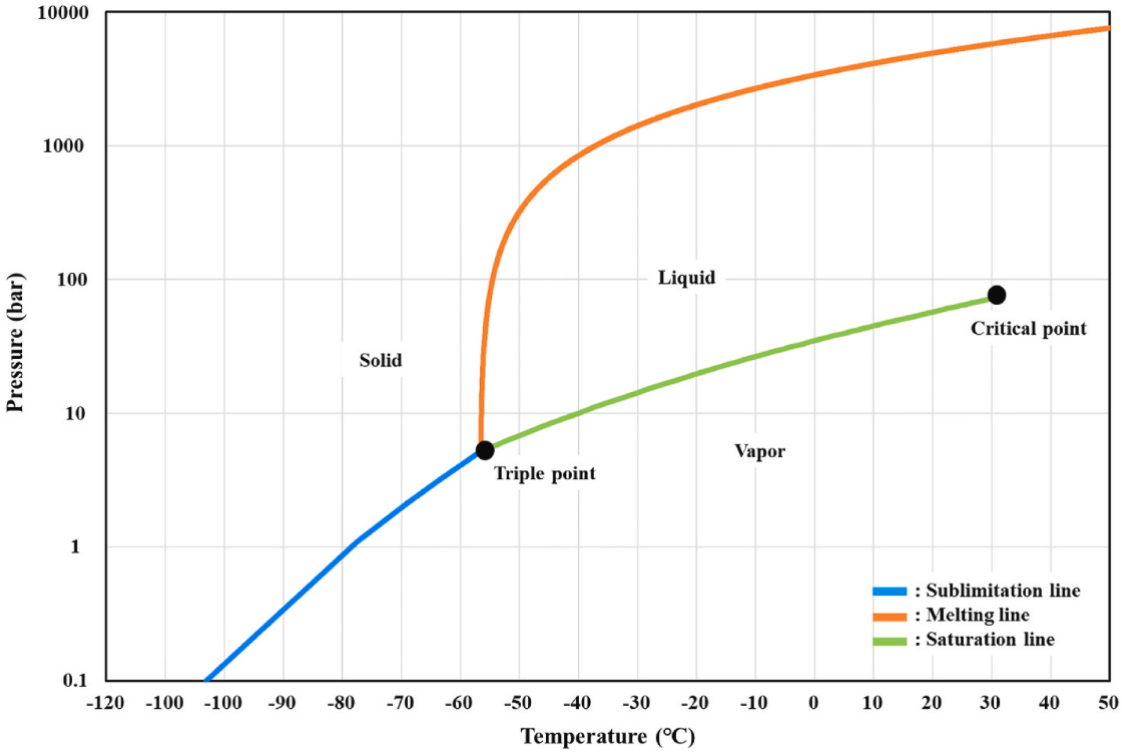

Fig. 5 P–T diagram of CO_2 (Lee et al., 2024)

enthalpy changes. It was designed to import the thermodynamic property data of each substance required for the calculations (e.g., thermal expansion coefficient, viscosity coefficient, and EOS) from Aspen Hysys.

3.1.1 Thermal homogeneous model (THM)

The THM determines each variable by solving thermodynamic differential equations that refer to a previous study (Peng and Ahluwalia, 2013) and converts them into functions for calculation. The model was designed to calculate the physical properties of the fluid in the tank at each time interval (Δt) by solving ordinary differential equations, Eqs. (2), (3), and (14):

$$\left(\frac{1}{\rho_v}-\frac{1}{\rho_l}\right)\frac{dm_v}{dt}=\left\{m_v\left[\frac{1}{(\rho_v)^2}\left(\frac{\partial\rho_v}{\partial T}\right)_P\right]+m_l\left[\frac{1}{(\rho_l)^2}\left(\frac{\partial\rho_l}{\partial T}\right)_P\right]\right\}\frac{dT}{dt}+\left\{m_v\left[\frac{1}{(\rho_{mrv})^2}\left(\frac{\partial\rho_v}{\partial P}\right)_T\right]+m_l\left[\frac{1}{(\rho_l)^2}\left(\frac{\partial\rho_l}{\partial P}\right)_T\right]\right\}\frac{dP}{dt} \quad (14)$$

Fig. 6 presents a schematic algorithm of the THM

3.1.2 Thermal two-zone model

A TTZM simulation was performed using the BoilFAST (Jusko et al., 2021). BoilFAST is open software that can rapidly calculate BOG by selecting the material composition, initial boundary conditions, and tank geometry. For CO_2, GERG-2008 is used as a state equation, and the model was constructed by setting various shapes and conditions of the tank.

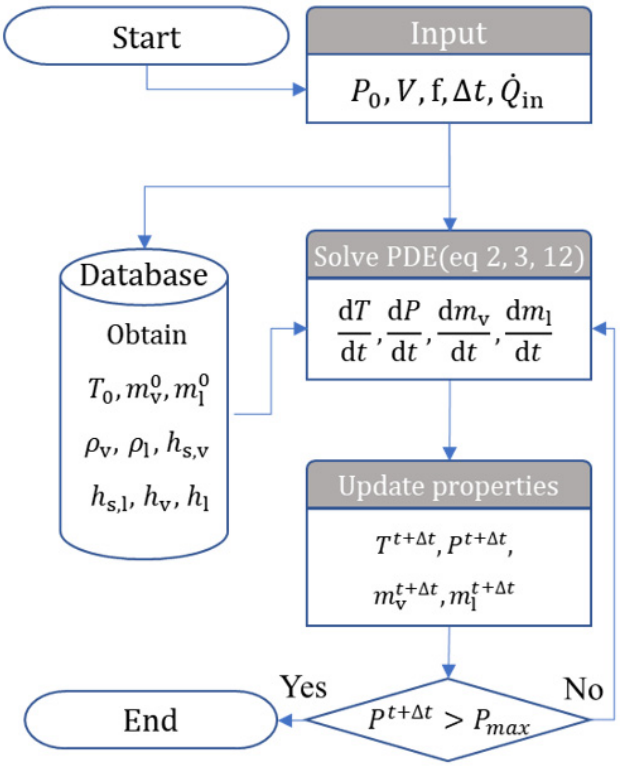

Fig. 6 Schematic algorithm of the THM

3.1.3 Thermal multi-zone model

The TMZM assumed that the total heat flow from the outside of the tank was divided into the gas and liquid by the parameter f as well as the gas cross-sectional area (A_v) and the liquid cross-sectional area (A_l) according to the tank geometry and liquid level (Eqs. (12) and (13)). The gas–liquid interface was considered saturated. Heat transfer from the gas to the interface and from the interface to the liquid was assumed, and the difference between the amount of heat introduced into the interface from the gas and the amount of heat introduced into the liquid from the interface was involved in vaporization. Vaporization was assumed to exist only at the interface, and the enthalpy remaining on the tank walls was not considered. The heat transfer between the interfaces (Q_{vs} and Q_{sl}) was calculated based on the properties of the gas region of the superheated vapor and the liquid region of the subcooled liquid, as shown in Eqs. (7) and (8). The mass flow at the interface can be calculated using Eq. (15).

$$\Delta m_s = \frac{(Q_{vs}-Q_{sl})}{(h_{s,v}-h_{s,l})}\Delta t \quad (15)$$

The calculated mass flow was used in the energy balance equations between the gas and liquid regions, as expressed in Eqs. (16) and (17).

$$\Delta h_v = (Q_v - Q_{vs} + \Delta m_s(h_{s,v}-h_v))\frac{\Delta t}{m_v} \quad (16)$$

$$\Delta h_l = (Q_l - Q_{sl} - \Delta m_s(h_{s,l}-h_l))\frac{\Delta t}{m_l} \quad (17)$$

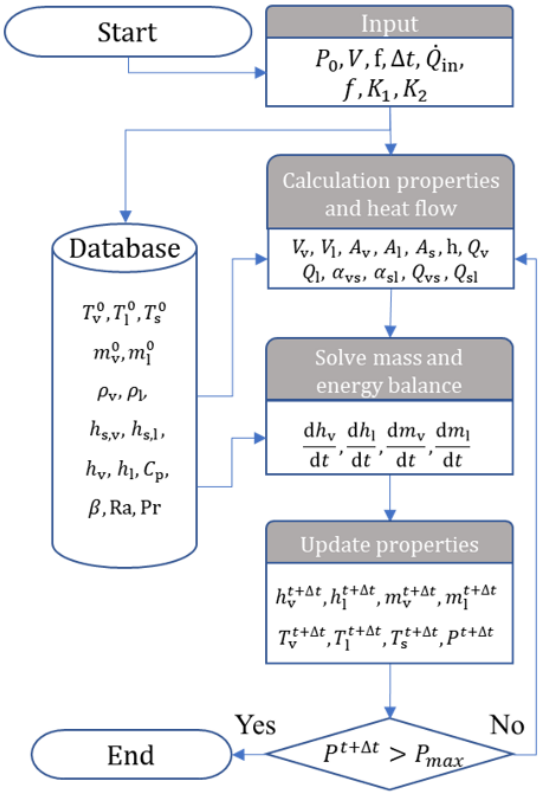

Fig. 7 Schematic algorithm of the thermal multi-zone model

The calculated enthalpy change determines the pressure of each region and completes the final calculation. Fig. 7 presents the schematic algorithm of TMZM.

3.2 Simulation

In this study, an LCO_2 simulation was performed, assuming that a number of vertical tanks with a capacity of 1,000 m^3 are used to store LCO_2. Among various types of tanks available for LCO_2 carriers, vertical tanks are more flexible in the internal arrangement of ships and have a benefit in terms of the amount of BOG because of the relatively small area of the gas-liquid interface, unlike horizontal tanks. They can also save installation, operation, and maintenance costs by assuming that LCO_2 is transported from the tank to the pump in a separate pump room rather than the installation of an immersible pump in each tank (Yoo et al., 2013).

Fixed values of such external heat for simulation must be assumed because the BOG generation and pressure increase in cryogenic liquid cargo are related directly to external heat. The boil-off rate (BOR) by the heat flow from the outside was assumed to be 0.1%/d based on the LCO_2 fully-laden condition in the tank (Al Ghafri et al., 2022), and the heat flow can be calculated using Eq. (18). Δh_{vap} is the evaporation heat of carbon dioxide and ρ_{CO_2} is its density:

$$BOR = \frac{\sum Q_{in}}{\rho_{CO_2} \times V_{CO_2} \times \Delta h_{vap}} \times 3600 \times 24 \times 100\% \quad (18)$$

Table 2 lists the initial state assumptions of the tank. The storage pressure of CO_2 was assumed to be 600 kPa, which is higher than the triple point, and the maximum allowable working pressure was 800 kPa. In addition, the storage of pure LCO_2 was assumed. The heat flow was assumed to be a fixed value to have the same BOR regardless of the tank geometry.

Table 2 Simulation tank conditions

Parameter	Value
Composition	100% CO_2
Volume (m^3)	1,000
Initial / Max pressure (kPa)	600/ 800
Boil off rate (%/d)	0.1
Heat flow (kW)	4.36
Filling ratio	0.95

3.3 Parameter Tuning

The TMZM presented in this study was designed to perform parameter optimization based on experimental data by reflecting the geometry of the tank. Determination of parameters is required for a self-pressurization simulation. TMZM determines the heat flow rates of the gas and liquid through the parameter f, as shown in Eq. (9). Kartuzova et al. (2015) proposed one as the most suitable value of f at a filling ratio of 90% for liquefied hydrogen storage tanks. Wang et al. (2022) presented $f = 0.5$ after estimating f through individual liquefied hydrogen experiments. TMZM can also set the parameters K_1 and K_2 that represent heat transfer at the interface, as expressed in Eqs. (12) and (13). Moreover, a previous study presented 0.1 as an appropriate value for liquefied hydrogen (Wang et al., 2022).

In this study, the parameters of the proposed model were optimized based on an experimental study on LCO_2 conducted for parameter setting. The experimental data used were based on the LCO_2 storage tank experiment by Yoo (2011), and Table 1 lists the specifications of the tank used in the experiment. The volume of the storage tank estimated from the specifications presented in the literature was approximately 2.17 m^3, and the heat flow was estimated to be 0.091 kW based on the given specifications. The experiment was performed for approximately 50,000 s.

For parameter optimization, in the first case, the values of K_1 and K_2 that minimize the root mean square error (RMSE) compared to the existing experimental pressure rise results were estimated while $f = 1$ was fixed, as listed in Table 3. In the second case, the K_1 and K_2 values that minimize the deviation of the liquid–gas temperature difference (approximately 23 K) in the experiment were estimated for $f = 1$. In the third case, the K_1 and K_2 values that minimizes the deviation of the liquid–gas temperature difference in the experiment were estimated for $f = 0.5$.

4. Result

4.1 THM and TTZM Simulation Result

In the simulation results, the THM and TTZM showed similar results for the self-pressurization caused by the heat flow from the outside. The THM showed a pressure holding time of approximately

Table 3 Summary of parameter tuning cases

Case	Model	Parameter		
		f	K_1, K_2	
1	TMZM	1	0.0152	Estimating K by minimizing the RMSE of the initial experiment temperature when $f = 1$.
2	TMZM	1	110	Estimating K to minimize the deviation of the final liquid-gas temperature difference in the experiment when $f = 1$.
3	TMZM	0.5	59	Estimating K to minimize the deviation of the final liquid-gas temperature difference in the experiment when $f = 0.5$.

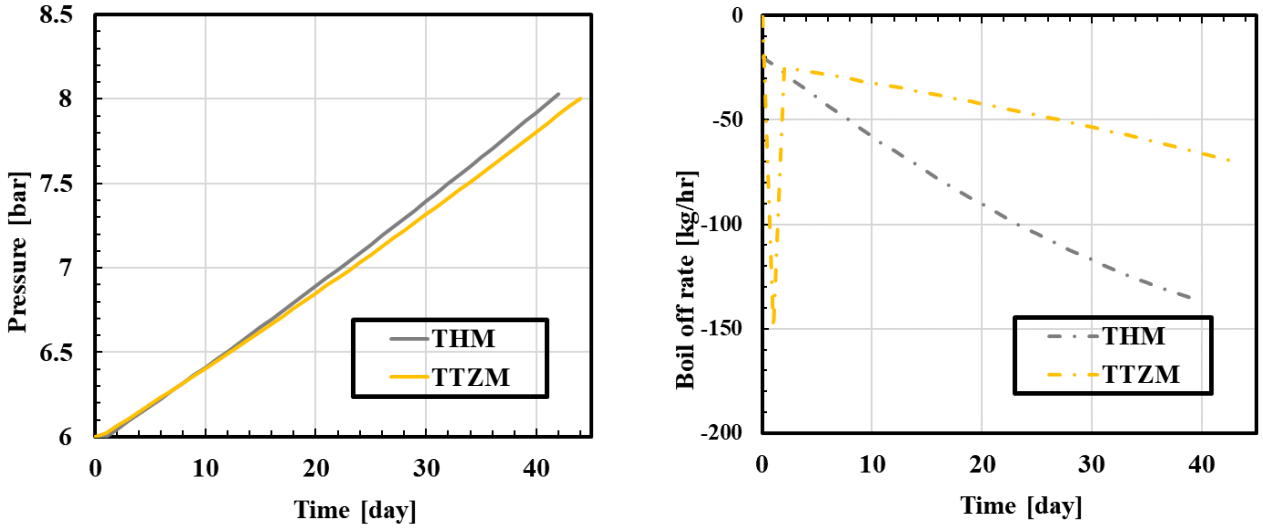

(a) (b)

Fig. 8 Result of (a) pressure build-up and (b) boil-off rate in large tank using the THM and TTZM

41 days for 600 to 800 kPa, and the TTZM showed a pressure holding time of approximately 42 days, as shown in Fig. 8(a). The two models, however, exhibited condensation rather than evaporation because the BOR is negative at all times during the storage period, as shown in Fig. 8(b). This result was attributed to the temperature of the liquid increasing as the pressure in the saturated state of the pure substance increased, and the required amount of heat consumes the heat of the gas phase as well as the heat introduced from the outside as energy. These results indicate the limitations of THM and TTZM, a non-equilibrium model. Consequently, the self-pressurization rate was estimated based on equilibrium, and the saturated liquid can be excessively slow compared to that observed in reality.

4.2 TMZM Simulation Result

Fig. 9 shows the parameter optimization results of case 1 that determines values to minimize RMSE from the pressure rise results of

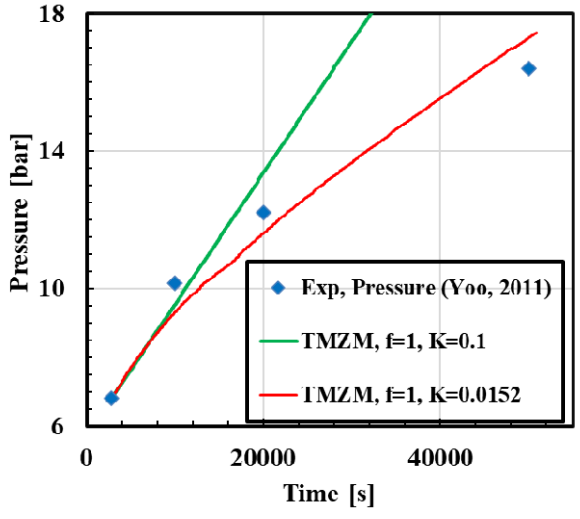

Fig. 9 Optimization result of the pressure build-up in a large tank using TMZM

TMZM at $f = 1$ based on the experiment results. The RMSE was lowest at K_1, $K_2 = 0.0152$ compared to the experimental values.

Table 4 and Fig. 10 show the results of the case 1 simulation performed based on the parameters determined for the LCO_2 storage condition on a ship (Table 1). The TMZM showed a relatively low pressure holding time of approximately 28 h for up to the maximum allowable working pressure (800 kPa), unlike previous THM and TTZM, as shown in Fig. 10(a). Condensation of the BOG did not occur, and the BOR increased gradually during the period with positive values, as shown in Fig. 10(b).

In the simulation result of case 1, however, the gas temperature increase was excessive. The temperature of the gas increased by more than 60 K during the pressure holding time (Fig. 10(c)), which is very high considering that the temperature of the liquid increased by 0.16 K during the same period (Fig. 10(d)). In particular, a comparison of the simulation and experiment results showed that the temperature was approximately 35 K higher than the highest temperature of the gas in the experiment (250 K; Yoo, 2011), and the temperature difference from the liquid was approximately 60 K. Therefore, the rapid increase in pressure inside the storage tank in the simulation was caused by an increase in the temperature of the gas suggesting that heat transfer was inhibited in the simulation results than that observed in reality. The experiment was performed for only a short time of 50,000 s. Consequently, very low heat transfer correction parameters (0.1 in the literature) of K_1, $K_2 = 0.0152$ were determined from parameter optimization to reproduce the rapid initial pressure rise. The heat transfer rate between the liquid and gas is underestimated if the heat transfer correction parameters decrease, as shown in Eqs. (7), (8), (12), and (13). The heat to be transferred to the liquid stays in the gas, which may lead to a rapid pressure increase inside the tank by increasing the enthalpy and temperature of the gas region.

Parameter optimization cases 2 and 3, which determine the parameters based on the temperature difference between the gas and

Table 4 Simulation results of the LCO_2 tank

Model	Initial / Terminated pressure (kPa)	Holding time (h)	Vapor Max. temperature (K)
Thermal homogeneous model (THM)	600 / 800	984	228
Thermal two-zone model (TTZM)		1008	230
Thermal multi-zone model (TMZM)		26	285

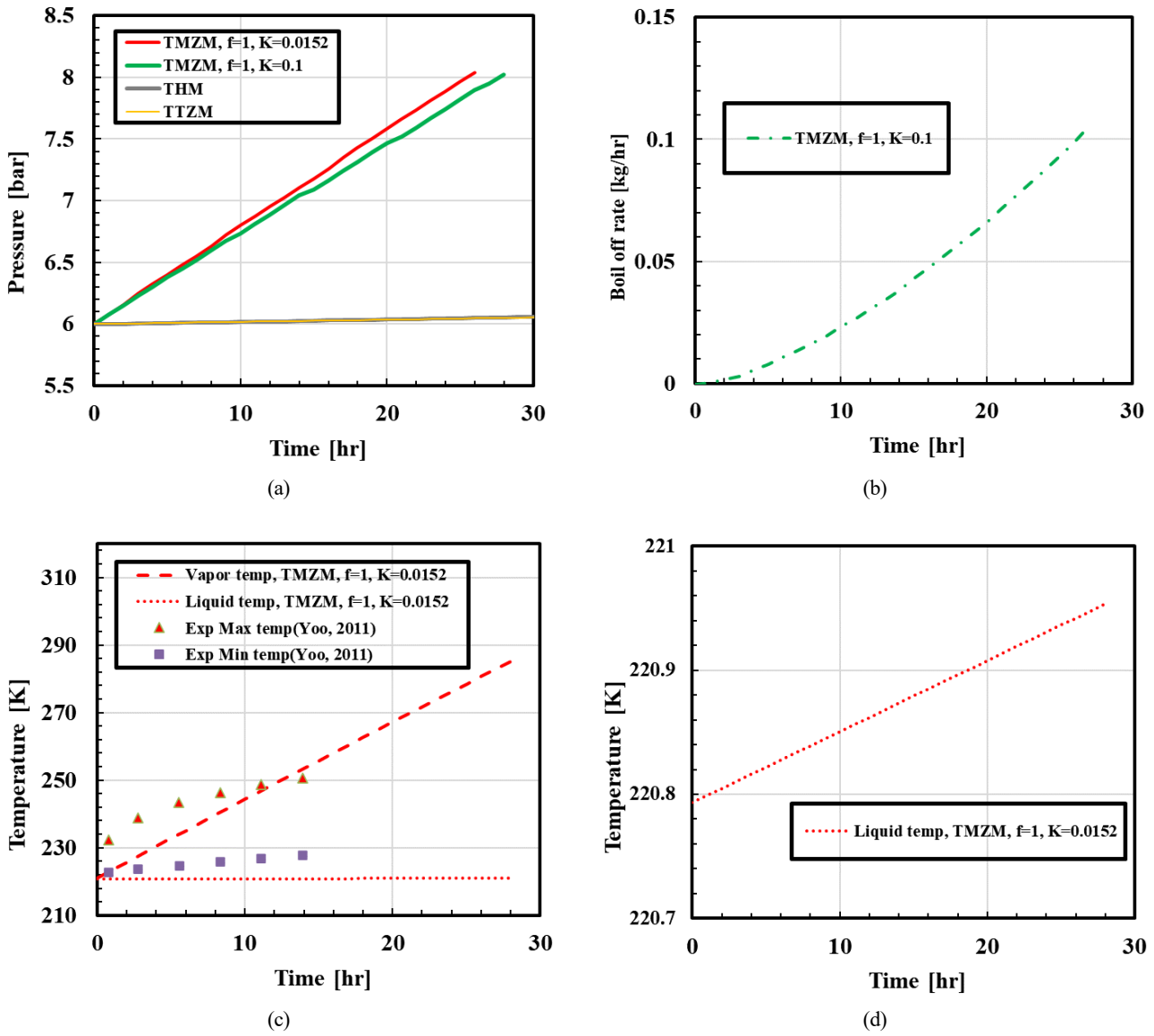

Fig. 10 Results of (a) pressure build-up in a large tank between three models and (b) vapor mass change, (c) temperature in TMZM (f = 1, K = 0.0152), (d) liquid temperature in TMZM (f = 1, K = 0.0152)

liquid in the experiment, were also performed to supplement these results. Based on the literature, optimization was performed in two cases where the gas–liquid heat flux ratio f was 1 (case 2) and 0.5 (case 3), respectively. Consequently, in case 2, the maximum temperature difference between the gas and liquid was 23 K, similar to the experiment for K_1, K_2 = 110. In case 3, K_1, K_2 = 59 resulted in the smallest difference. f = 1 and K_1, K_2 = 110 exhibited a pressure holding time of approximately 318 h (approximately 13 days) while f = 0.5 and K_1, K_2 = 59 showed a holding time of approximately 285 h (approximately 12 days) in the simulation results (Fig. 11(a) and 11(b)).

In the optimization of cases 2 and 3, the heat transfer correction parameters were higher than in case 1 to reduce the temperature difference between the gas and liquid. This led to active heat transfer between the gas and liquid in the simulation, reducing the increase in the temperature and enthalpy of the gas and decreasing the pressure increase rate. In other words, the rapid pressure increase in the case 1 optimization results is the result of the excessive temperature rise in the

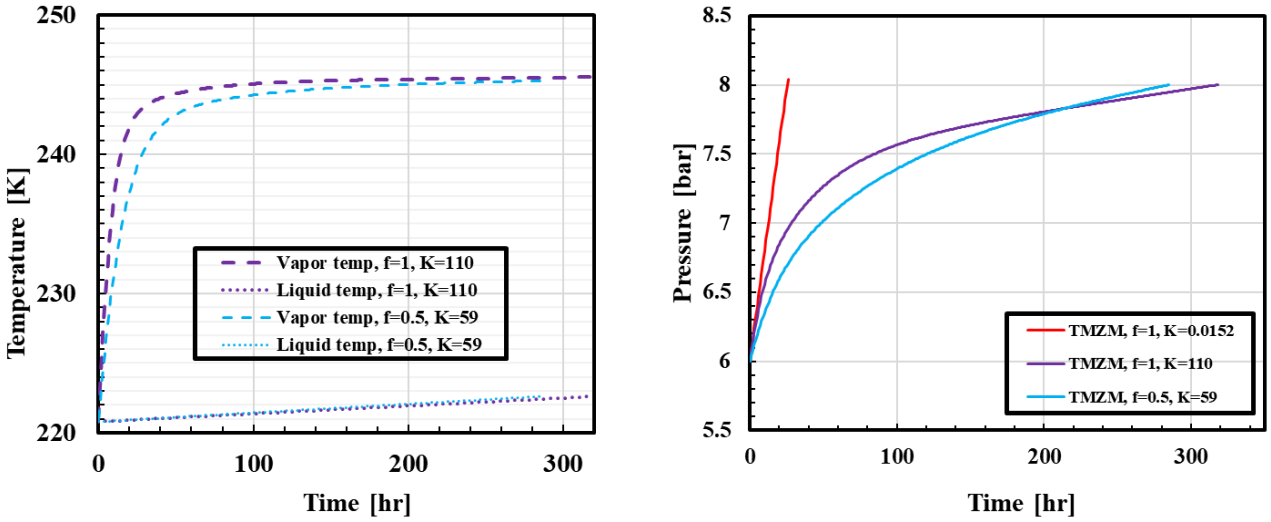

(a) (b)

Fig. 11 Results of (a) vapor and liquid temperature in the 2nd and 3rd parameters tuning and (b) pressure build-up using TMZM with optimization

gas region and the inhibited heat transfer between the gas and liquid. The optimization results for cases 2 and 3 suggest that the pressure rise was delayed because of the reduction in the temperature increase rate of the gas region and more active heat transfer. Consequently, the self-pressurization rate was dominantly affected by the temperature increase of the gas region, and the pressure holding time is expected to increase as gas–liquid heat transfer becomes more active by approaching equilibrium. On the other hand, the holding time was expected to decrease as the gas–liquid heat transfer becomes less active.

This study did not reflect phenomena that occur during actual operation, such as BOG removal, hull motions, and sloshing, and the assumption that vaporization occurs only at the interface inside the tank may result in differences from the phenomena that occur in actual transport. Furthermore, verification is required through experiments on the pressure increase of actual low-temperature LCO_2. These limitations need to be reflected in further research.

5. Conclusion

In this study, a simulation was performed using three different thermodynamic models for the self-pressurization of LCO_2 at 600 kPa to predict the pressure-holding time of LCO_2. The thermal homogeneous model (THM) is based on the gas-liquid equilibrium, and the thermal two-zone model (TTZM) simulates the saturated liquid and superheated vapor. The LCO_2 tank had a holding time of up to 42 days. The liquid of the THM and TTZM, however, received a large amount of thermal energy from the gas to maintain the saturated state, and the BOR remained negative throughout the entire simulation period, resulting in condensation rather than evaporation. Hence, the holding time prediction results of an equilibrium-based model can be much longer than that observed in reality. The simulation results that used the thermal multi-zone model (TMZM) showed that the first optimization case ($f = 1$, K_1, $K_2 = 0.0152$) that performed parameter optimization based on the tank experiment result data revealed a holding time of only 26 h, but the result appears to be unrealistic because the temperature difference between the gas and liquid was more than 60 K. This is because heat transfer was excessively inhibited as the heat transfer parameters K_1 and K_2, which were adjusted to simulate the rapid initial temperature rise in the experiment, were too low. The predicted holding time can be excessively shorter than in reality. These results were improved by performing the second and third optimizations based on the temperature difference from the experiment. Consequently, the second optimization case ($f = 1$, K_1, $K_2 = 110$) showed a holding time of 318 h (approximately 13 days), and the third optimization case ($f = 0.5$, K_1, $K_2 = 59$) revealed a holding time of approximately 285 h (approximately 12 days). These results suggested that the holding time can be significantly different depending on the heat transfer phenomenon between the gas and liquid. These results are expected to be helpful in predicting the pressure increase in the storage tanks on LCO_2 carriers.

Conflict of Interest

Youngsub Lim serves as an editorial board member of the Journal of Ocean Engineering and Technology, but he had no role in the decision to publish this article. No potential conflict of interest relevant to this article was reported.

Funding

This research was supported by Korea Institute of Marine Science & Technology Promotion(KIMST) funded by the Ministry of Oceans and Fisheries(2520000243), and the Korea Research Institute of Ships and

Ocean engineering, grant from Endowment Project of "Technology Development of Onboard Carbon Capture and Storage System and Pilot Test" funded by Ministry of Oceans and Fisheries (PES5110). The Research Institute of Marine Systems Engineering and Institute of Engineering Research at Seoul National University provided research facilities.

References

Al Ghafri, S. Z., Swanger, A., Jusko, V., Siahvasho, A., Perez, F., Johns, M. L., & May, E. F. (2022). Modelling of liquid hydrogen boil-off. *Energies, 15*(3), 1149. https://doi.org/10.3390/en15031149

Aspelund, A., Mølnvik, M. J., & De Koeijer, G. (2006). Ship transport of CO_2: Technical solutions and analysis of costs, energy utilization, exergy efficiency and CO_2 emissions. *Chemical Engineering Research and Design, 84*(9), 847−855. https://oi.org/10.1205/cherd.5147

Barsi, S., & Kassemi, M. (2008). Numerical and experimental comparisions of the self-pressurization behavior of an LH2 tank in normal gravity. *Cryogenicsm 48*(3−4), 122−129. https://doi.org/10.1016/j.cryogenics.2008.01.003

Cheon, B. H., Bang, K. J., Ki , H. G., Han, S. K., Hwang, Y. S., & Park, S. G. (2023). The development of a vertically asymmetric bi-lobe tank for large-scale LCO2 carrier. In *33rd International Ocean and Polar Engineering Conference* (ISOPE-I-23-503). ISOPE.

Clark, D. E., Oelkers, E. H., Gunnarsson, I., Sigfússon, B., Snæbjörnsdóttir, S. Ó., Aradottir, E. S., & Gíslason, S. R. (2020). CarbFix2: CO_2 and H_2S mineralization during 3.5 years of continuous injection into basaltic rocks at more than 250 C. *Geochimica et Cosmochimica Acta*, *279*, 45−66. https://doi.org/10.1016/j.gca.2020.03.039

Hastings, L. J., Flachbart, R. H., Martin, J. J., Hedayat, A., Fazah, M., Lak, T., Nguyen, H., & Bailey, J. W. (2003). *Spray bar zero-gravity vent system for on-orbit liquid hydrogen storage* (No. NASA/TM-2003-212926).

Hegerland, G., Jørgensen, T., & Pande, J. O. (2005). - Liquefaction and handling of large amounts of CO_2 for EOR. In *Greenhouse Gas Control Technologies 7* (pp. 2541−2544). Elsevier Science Ltd. https://doi.org/10.1016/B978-008044704-9/50369-4

Holman, J. P. (2002). *Heat transfer* (9th ed.). McGraw-Hill.

Jung J, & Seo Y. (2022). Onboard CO_2 capture process design using rigorous rate-based model. *Journal of Ocean Engineering and Technology, 36*(3), 168−180. https://doi.org/10.26748/KSOE.2022.006

Jusko, V., Al Ghafri, S. Z.S., May, E.F. (2021). *Fluid Sciences and Resources Division* (BoilFAST v1.1.0). The University of Western Australia:Perth, Australia.

Kartuzova, O. V., Kassemi, M., Moder, J. P., & Agui, J. H. (2014). Self-pressurization and spray cooling simulations of the multipurpose hydrogen test bed (MHTB) ground-based experiment. In *50th AIAA/ASME/SAE/ASEE Joint Propulsion Conference* (AIAA 2014-3578). https://doi.org/10.2514/6.2014-3578

Kearns, D., Liu, H., & Consoli, C (2021). *Technology readiness and costs of CCS*. Global CCS institute, 3.

Kim, S., Lee, J. G., Kim, S., Heo, J., Bang, C. S., Lee, D. K., Lee, H., Park, G ., Lee, D. Y., & Lim, Y. (2024). Experiment and simulation of LNG self-pressurization considering temperature distribution under varying liquid lecel. *Energy, 290*, 130071. https://doi.org/10.1016/j.energy.2023. 130071

Kongsiorden, H., Kårstad, O., & Torp, T. A. (1998). Saline aquifer storage of carbon dioxide in the Sleipner project. *Waste Management, 17*(5−6), 303−308. https://doi.org/10.1016/S0956-053X(97)10037-X

Lee, J., Son, H., Oh, J., Yu, T., Kim, H., & Lim, Y. (2024). Advanced process design of subcooling re-liquefaction system considering storage pressure for a liquefied CO_2 carrier. *Energy*, *293*, 130556. https://doi.org/10.1016/j.energy.2024.130556

Matveev, K. I., & Leachman, J. W. (2023). The effect of liquid hydrogen tank size on self-pressurization and constant-pressure venting. *Hydrogen, 4*(3), 444−455. https://doi.org/10.3390/hydrogen4030030

Nellis, G., & Klein, S., (2009). *Heat transfer.* Cambridge University Press.

Peng, J. K., & Ahluwalia, R. K. (2013). Enhanced dormancy due to para-to-ortho hydrogen conversion on onsulated cryogenic pressure vessels for automotive applications. *International journal of hydrogen energy, 38*(31), 13664−13672. https://doi.org/10.1016/j.ijhydene.2013.08.039

Rotenberg, Y. (1986). Numerical simulation of self pressurization in a small cryogenic tank. In *Advances in Cryogenic Enfinerring: Volume 31* (pp. 963−971). Bostion, MA: Speinger US.

Seo, M., & Jeong, S. (2010). Analysis of self-pressurization phenomenon of cryogenic fluid storage tank with thermal diffusion model. *Cryogenics, 50*(9), 549−555. https://doi.org/10.1016/j.cryogenics.2010.02.021

Wang, H. R., Wang, B., Pan, Q. W., Wu, Y.Z., Jiang, L., Wang, Z. H., & Gan, Z. H. (2022). Modeling and thermodynamic analysis of thermal performance in self-pressurized liquid hydrogen tanks, *International Journal of Hydrogen Energy, 47*(71), 30530−30545. https://doi.org/10.1016/j.ijhydene.2022.07.027

Yoo, B. Y. (2011). *An experimental study on the thermocline layer in a cargo tank of CO_2 carriers* [Doctoral dissertation, Seoul National University]. https://www.riss.kr/link?idT12406961

Yoo, B. Y., Choi, D. K., Kim, H. J., Moon, Y. S., Na, H. S., & Lee, S. G. (2013). Development of CO_2 terminal and CO_2 carrier for future commercialized CCS market. *International Journal of Greenhouse Gas Control, 12*, 323−332. https://doi.org/10.1016/j.ijggc.2012.11.008

Zhu, S., Li, Y., Zhi, X., Gu, C., Tang, Y., & Qiu, L. (2020). Numerical analysis of nitrogen condensation heat transfer enhancement with liquid film fluctuation at cryogenic temperature. *International Journal of Heat and Mass Transfer, 149*, 119151. https://doi.org/10.1016/j.ijheatmasstransfer.2019.119151

Zuo, Z., Wu, J., & Huang, Y. (2021). Validity evaluation of popular liquid-vapor phase change models for cryogenic self-

pressurization process. *International Journal of Heat and Mass Transfer, 181*, 121879. https://doi.org/10.1016/j.ijheatmasstransfer.2021.121879

Author ORCIDs

Author name	ORCID
Nam, Taehun	0009-0008-1488-5854
Yu, Taejong	0009-0005-7714-5843
Lim, Youngsub	0000-0001-9228-0756